M. BRAMOWICZ[*], S. KULESZA[**], P. CZAJA[***], W. MAZIARZ[***]

APPLICATION OF THE AUTOCORRELATION FUNCTION AND FRACTAL GEOMETRY METHODS FOR ANALYSIS OF MFM IMAGES

ZASTOSOWANIE FUNKCJI AUTOKORELACJI ORAZ GEOMETRII FRAKTALNEJ DO ANALIZY OBRAZÓW STRUKTUR DOMENOWYCH REJESTROWANYCH METODĄ MFM

Presented work is focused on the use of correlation methods for numerical analysis of magnetic stray field over the surface of materials. Obtained results extend our previous findings about application of the autocorrelation function and the fractal analysis for characterization of magnetic surfaces. Several domain images are recorded at various tip-sample gaps (i.e. the lift heights), and then their average widths were extrapolated down to the zero distance in order to estimate the width seen right on the surface. Apart from that, fractal parameters were derived from autocorrelation function, which turned out to be sensitive to the lift height, and might constitute universal measure (the critical lift height), above which the MFM signal became dominated by thermal noises and non-magnetic residual interactions.

Keywords: Atomic Force Microscopy, Magnetic Force Microscopy, magnetic domains, fractal analysis

Niniejsza praca dotyczy zastosowania metod korelacyjnych do numerycznej analizy obrazów rozkładu pola magnetycznego emitowanego z obszarów spontanicznego namagnesowania. W pracy przedstawiono kontynuację badań nad zastosowaniem funkcji autokorelacji oraz metod analizy fraktalnej w badaniach struktury domenowej oraz charakterystyki emitowanego z nich pola magnetycznego.

Wyniki badań wykazują zależność mierzonej metodami mikroskopii sił magnetycznych (MFM) szerokości domen od wysokości skanowania nad badaną powierzchnią, sugerując przeprowadzanie serii pomiarów na różnych wysokościach (h), ich aproksymację z następną ekstrapolacją do powierzchni (h=0). Przeprowadzona analiza fraktalna, wskazuje na możliwość jej aplikacji do charakterystyki zmian sygnału magnetycznego rejestrowanego przez MFM. Pozwala ona również na wyznaczenie wysokości krytycznej (h_{kr}), na której sygnałem dominującym stają się nakładające się na sygnał magnetyczny pozostałości niemagnetycznych interakcji między igłą sondy i badaną powierzchnią, stanowiące rejestrowany przez MFM szum.

1. Introduction

Magnetic Force Microscopy (MFM) is a secondary operation mode derived from the Scanning Probe Microscopy (SPM) to image the spatial variation of the magnetic stray fields above the studied surface. Basically, SPM makes use of the van der Waals forces well described by a Lennard-Jones potential [1] occurring between the tip and the surface to image the surface topography. These van der Waals forces are limited to several atoms placed at the very end of the tip and on the surface straight below. However, with increasing tip-surface distance other interactions become significant, such as: magnetic, electrostatic, and capillary ones.

MFM employs sharp silicon tips coated with thin ferromagnetic films (Fig. 1). To separate the effects of magnetic forces from those of the mechanical ones, the measurements are carried out using a two-pass method, in which the sample is scanned twice. In the first pass, the probe tip is oscillating with the frequency slightly above the resonance (f_0), and lightly taps the sample surface. With varying tip-sample distance, the van der Waals forces change the cantilever's oscillation amplitude, which is used to map the surface topography. In the second pass, the tip is lifted from tens to hundreds of nanometers above the surface (Fig. 1) and follows the topography line equal to constant van der Waals force, and hence maintaining constant tip-sample distance. Since MFM is used primarily to image magnetic domains, that is the size and shape of spontaneously magnetized structures in the near subsurface, the lift height needs to be large enough in order to diminish the effect of the dipole interactions. Providing that the van der Waals forces acting on the tip remain constant during the second pass, any change in the cantilever's oscillation amplitude can be related to the gradient of the magnetic force. Apart from that, however, the phase shift between the cantilever's oscillation relative to the piezo drive occurs as well, according to [2, 3]:

[*]   UNIVERSITY OF WARMIA AND MAZURY IN OLSZTYN, FACULTY OF TECHNICAL SCIENCES, OCZAPOWSKIEGO 11, 10-719 OLSZTYN, POLAND

[**]   UNIVERSITY OF WARMIA AND MAZURY IN OLSZTYN, FACULTY OF MATHEMATICS AND COMPUTER SCIENCE, SLONECZNA 54, 10-710 OLSZTYN, POLAND

[***]   INSTITUTE OF METALLURGY AND MATERIALS SCIENCE POLISH ACADEMY OF SCIENCE, REYMONTA 25, 30-059 KRAKÓW, POLAND

$$\Delta\Phi = \frac{Q}{k}\left(q\frac{\partial H_z}{\partial z} + m_x\frac{\partial^2 H_x}{\partial z^2} + m_y\frac{\partial^2 H_y}{\partial z^2} + m_z\frac{\partial^2 H_z}{\partial z^2}\right) \quad (1)$$

where: $\Delta\Phi$ – the phase shift of the cantilever's oscillation, Q – the quality factor of the MFM tip, k – the spring constant of the cantilever, q – effective magnetization of the probe's tip, m_x, m_y, m_z – the components of the magnetic moment of the MFM tip along X, Y, and Z axis, respectively, H_x, H_y, H_z – the components of the stray magnetic field above the surface.

The phase shift signal recorded at discrete points on the surface mesh is stored in the form of a 2-dimensional array representing spatial variations of the magnetic field. Observed interaction forces depend on several factors including, among others: geometry of the tip and the surface that affects effective overlap of their magnetic fields, magnetic stray field intensity, the coercivity and the magnetic moment of the probe's tip, and contribution of non-magnetic forces (capillary, electrostatic) other than previously mentioned dipole forces [4,5]. Apart from that, however, the largest contribution comes from the magnetization of the tip's coating. Some changes in that aspect are possible by proper choice of the MFM probe for specific application, and by magnetizing the tip with a strong permanent magnet prior to the measurement. On the other hand, the control over the processes of demagnetization and remagnetization of the tip's magnetic coating when the probe scans over the surface is highly unlikely.

As mentioned previously, another key parameter is the lift height h at which the normal component of the gradient of the magnetic stray field above the surface is probed by the tip while it is moving in the second pass. The effect of the lift height on the magnitude of magnetic interactions is schematically drawn in Fig. 1, which shows that the larger h value corresponds to a smaller overlap between the stray field and the magnetic field emitted from the tip's coating.
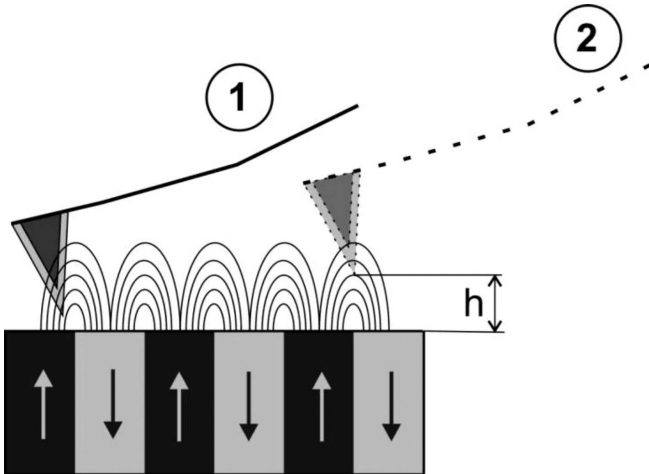

Fig. 1. The effect of the lift height on the effective interaction between the magnetic stray field above the surface and the magnetic field emitted by the probe's tip

A large number of studies on the analysis of the MFM results have been published so far, however, most of them were concerned about the issues of visual, and statistical interpretation of obtained phase shift maps together with the determination of the actual shape of the magnetic domains. Our goal is to extend the prospects of the MFM measurements making use of the autocorrelation function and fractal geometry to study the dynamics of the decay of the fluctuations of the magnetic stray field along normal to the surface.

2. Theory

In order to estimate the widths of the cross-sectional profiles of observed magnetic field fluctuations that correspond roughly to the widths and lengths of the magnetic domains, the autocorrelation function was used in the form [6]:

$$R(k,l) = \frac{1}{MN}\sum_{x=0}^{M-1}\sum_{y=0}^{N-1}[z(x,y) - x_z][z(x+k,y+1) - x_z] \quad (2)$$

where: M, and N – are the numbers of the scan steps along X and Y axis, respectively, (x, y) – discrete Cartesian coordinates of a given point on the MFM image, z(x, y) – the phase shift value measured at (x, y), whereas x_z – the mean phase shift of the cantilever's oscillation relative to piezo drive given by:

$$x_z = \frac{1}{MN}\sum_{x=0}^{M-1}\sum_{y=0}^{N-1}z(x,y) \quad (3)$$

As such, the autocorrelation function is widely used for analysis of the surface properties of materials, including topography features, texture, periodicity, and anisotropy ratio [6,7]. In terms of presented MFM measurements, this function describes spatial dependence between the phase shifts in the magnetic signal observed in various locations above the surface, which is assumed to be associated with the collective behavior of neighboring surface sites within magnetic domains coupled together with the exchange interaction.

Given R(k, l) results in the form of the autocorrelation maps, the main anisotropy axes (a_1, a_2) of the magnetic domains could be determined, and on that basis both the anisotropy ratio S_{tr}, and the mean width <W> of the domains could be subsequently estimated. The anisotropy ratio is derived according to the formula:

$$0 < S_{tr} = \frac{\tau_{a1}}{\tau_{a2}}\Big|_{R=1\to0,2} \leqslant 1 \quad (4)$$

where: τ_{a1}, and τ_{a2} – are the autocorrelation decay lengths along the fastest and the slowest decay directions, respectively, measured for R values falling from 1 down to 0.2. The domain width is assumed to be equal to the FWHM (Full Width at Half-Maximum) of the central peak in the autocorrelation spectrum [8]. An example of magnetic domains structure measured with lift height equal to 100 nm, and its autocorrelation map with main anisotropy axes marked as a_1, and a_2, are shown respectively in: Fig. 2(a), Fig. 2b. In addition, Fig. 2(c) schematically depicts the procedure of the mean profile width estimation. Note that the autocorrelation maps R(k, l) of perfectly isotropic surface structures (taken as a reference), need to have the form of a right cone with the anisotropy ratio S_{tr} = 1 [6, 7].
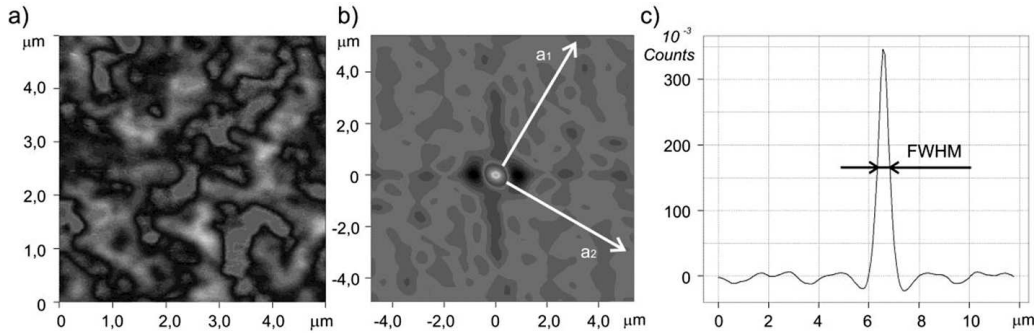
Fig. 2. (a) MFM domains structure of maraging steel, (b) Autocorrelation map obtained from MFM phase shift signal with main anisotropy axes along the fastest and the slowest function decay depicted as a1, and a2, respectively, (c) Autocorrelation profile along an arbitrary direction, from which the magnetic domain width is estimated

As mentioned previously, MFM measurements with zero lift height (i.e. with the average tip-surface distance equal to the oscillation amplitude) are highly unlikely due to significant contribution of non-magnetic short-range forces. On the other hand, obtained MFM maps of the phase shifts of the cantilever's oscillations relative to the piezo drive exhibit actually the boundaries of the domain structures in cross-sectional views at various heights above rather than right on the surface. According to that, we propose a simple method for estimating accurate boundaries of magnetic domains given their respective FWHM widths obtained for the lift heights varying from h_{min} to h_{max}. In the next step, a nonlinear regression is used to fit the power function of the variable h to the data. Finally, extrapolation of obtained fit down to zero results in the required average width of the magnetic domains right on the surface.

Application of fractal analysis for description of the magnetic domain structures was discussed in our recent paper [8] that presented MFM data recorded at constant lift height in the samples of maraging steels. Obtained results were concluded that the domain structure could be unambiguously characterized in terms of fractal parameters such as: the fractal dimension D, the topothesy Λ, and the corner frequency f_c, providing that the scan size is large enough to image at least a single domain. To extend these observations into wider perspective, current paper not only provides another results on the fractal structure of the magnetic properties, but is mostly aimed at studying the dynamics of the magnetic stray field decay along normal to the surface.

Fractal analysis was carried out using the structure function S(k, l) derived from the autocorrelation function according to the formula:

$$S(k, l) = 2\left(\sigma^2 - R(k, l)\right) \quad (5)$$

where: σ^2 – is the variance of the phase shift signal. Averaged along different scan directions, three-dimensional S(k, l) maps turned into two-dimensional profiles $S(\tau)$, from which the fractal parameters could be determined using numerical fit. Fig. 3 shows example log-log plot of the structure function together with the results of such a fit procedure.

In the profile structure function shown in Fig. 3, two parts can be distinguished. For small correlation lags τ, $S(\tau)$ follows the power law according to the formula [6, 9]:
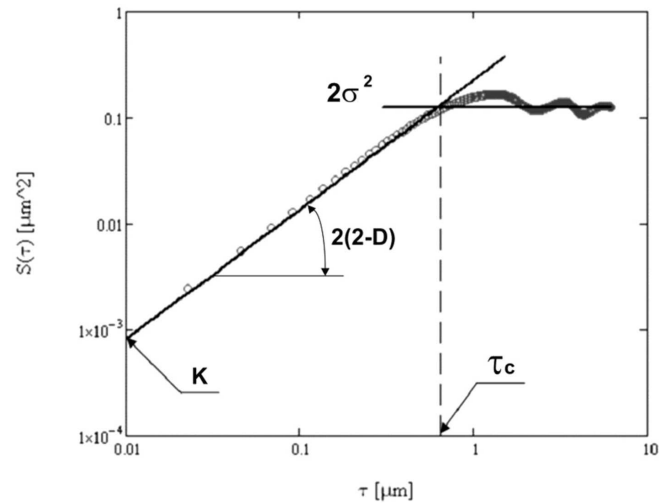

Fig. 3. Example log-log plot of the profile structure function schematically depicting the method of estimation of the fractal parameters

$$S(\tau) = \Lambda^{2(D-1)}\tau^{2(2-D)} \quad (6)$$

where: D – is the profile fractal dimension falling in the range from 1 to 2, while Λ – is the topothesy being equivalent to the distance between nearest-neighbor points on the surface inclined at an angle 1 rad [6]. Unfortunately, the topothesy itself has limited importance since it usually takes extremely small values, well below the instrumental resolution and even the inter-atomic distance, and hence the topothesy is usually combined together with the fractal dimension to define the parameter K [10]:

$$K = \frac{\pi G^{2(D-1)}}{2\Gamma(5 - 2D)\sin[(2 - D)\pi]} \quad (7)$$

where: G – is the scale-dependent constant, while Γ – is the Euler's function. In such a case, the profile structure function is given as:

$$S(\tau) = K\tau^{2(2-D)} \quad (8)$$

On the other hand, the profile structure function goes asymptotically towards the $2\sigma^2$ limit for large correlation lags τ. As seen in Fig. 3, the threshold on the $S(\tau)$ plot between the power-law behavior and the asymptotic behavior establishes the critical τ_c value referred to as the corner frequency τ_c [6].

3. Experiment

To study the dynamics of the magnetic stray field decay along normal to the surface, fractal analysis was applied to MFM data taken at the lift heights varying from 100 up to 1000 nm above the sample. The samples were cut from X2CoCrMoAl20-15-3 forged, thermally annealed martensitic steel rods with a square cross-section (120×120 mm^2). The annealing at 1050°C was carried out for 30 min, followed by the cooling in water down to the room temperature. XRD analysis performed after that treatment exhibited the crystal structure composed of original martensite with small addition of alloy carbides. In order to minimize the effect of the surface roughness (MFM resolution is basically limited by the tip curvature and the surface roughness), the sample was polished mechanically to obtain σ_{RMS} in the range 20-50 nm.

The measurements were carried out using Multimode 8 microscope with Nanoscope V controller (Bruker). The images were recorded while scanning with the MESP probes (Bruker) with the tip curvature radius about 35 nm, and the coercivity 400 Oe. The tip was scanning over a 20x20 μm^2 square area at 256 equidistant points along each scan axis. Prior to the measurements, the tip was magnetized along its vertical axis with a strong permanent magnet in order to increase the magnetic interaction with the surface.

Fig. 4 shows the topographic image of the surface measured in the first pass. The figure exhibits small precipitations of unknown origin (500 nm in diameter, up to 200 nm in height) firmly attached to the underlying base surface. These are probably carbide particles, which are much harder than surrounding martensitic structure. When polished, hard residual particles remained relatively intact with regard to otherwise soft martensite, which in contrast was largely destroyed. As a result, the treatment left the precipitated carbide stick out of the bulk solid.
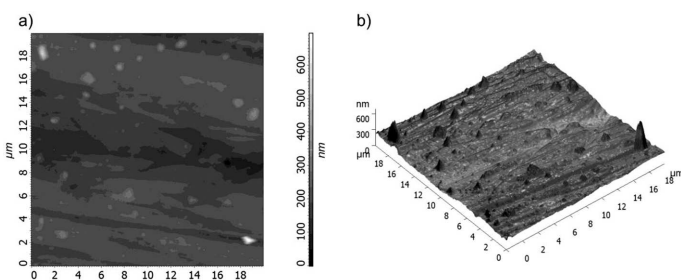

Fig. 4. The topographic image of the sample surface scanned in a first pass of the MFM measurement using the tapping mode

As mentioned previously, the MFM measurements of the surface shown in Fig. 4 were completed at 14 different lift heights, in the range from 100 up to 1000 nm. Obtained results concerning the spatial distributions of the magnetic phase shifts over the scan area are presented in Fig. 5. At first, the changes in the image contrast can be seen despite the diminishing signal amplitude, since the dynamically-scaled color palette exhibits increasing contribution of negative phase shifts with respect to positive ones with the lift height raising to 750 nm (Fig. 5(e)). For comparison, Fig. 6 presents the same images, although re-plotted using the absolute-scale color palette

to illustrate the effect of the signal decay with increasing lift heights.

MFM images recorded at lower lift heights provide the domain structure composed of randomly oriented thin stripes, 1÷4 μm in length. Random spatial orientation of the spontaneously magnetized domains expressed in terms of the anisotropy ratio suggests that magnetic properties of the steel sample are independent of the surface orientation. The anisotropy ratio was determined according to Eq. (4), given the plots of the autocorrelation function R(k, l) along the main anisotropy axes (a$_1$, a$_2$). Example plot of the R(k, l) recorded at the lift height of 100 nm is presented in Fig. 2.
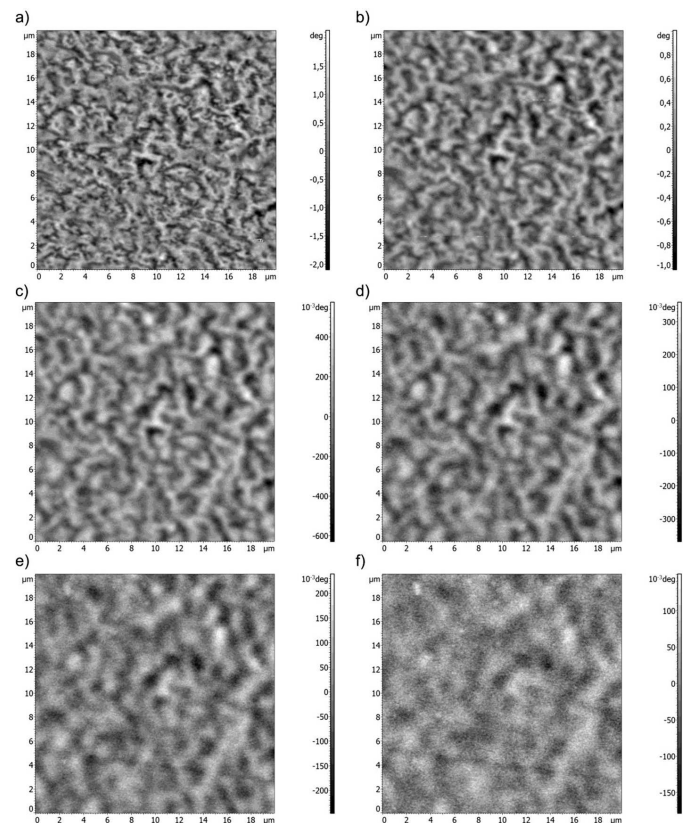

Fig. 5. Example MFM images measured over the surface shown in Fig. 4 at the lift heights equal to: a) 100 nm; b) 250 nm; c) 400 nm; d) 550 nm; e) 750 nm; f) 1000 nm. Note that the images are plotted using dynamically-scaled color palette to obtain the best possible contrast

In this case, the central peak exhibits elliptic cross-section with a low eccentricity, which also confirms isotropy in magnetic characteristics. The anisotropy ratio estimated at h = 100 nm, according to the method described in [8], appeared to be 0.848, consistent with our previous results published in [8], where S$_{tr}$ equal to 0.833 was found from measurements performed at the same lift height, but with larger scan size (5-50 μm).

In the whole range of the lift heights, measured phase shift of the magnetic signal falls down monotonically from around 4.5° at 100 nm to 0.3° at 1 μm over the surface. Observed changes in the maximum values of the phase shifts and respective RMS values of their variations are shown in Fig. 7.
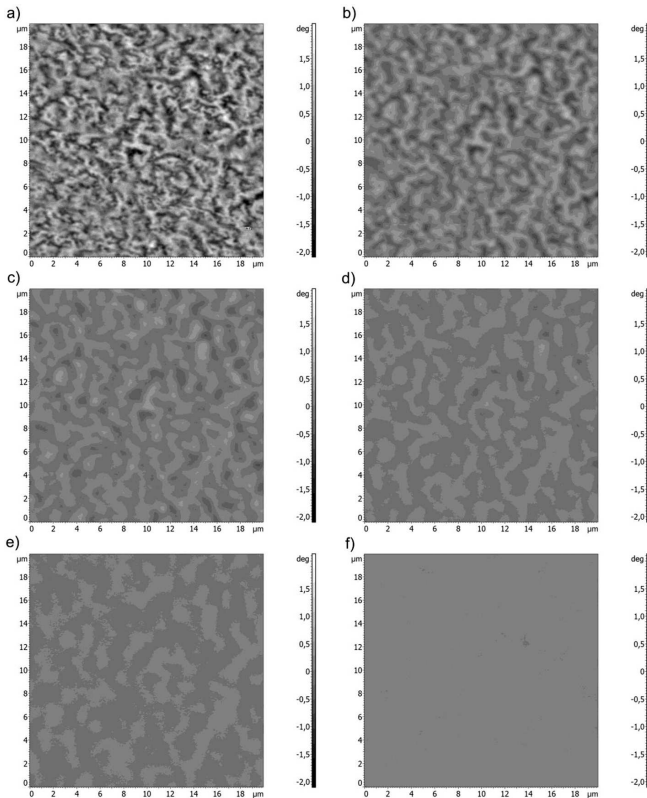
Fig. 6. Example MFM images measured over the surface shown in Fig. 4 at the lift heights equal to: a) 100 nm; b) 250 nm; c) 400 nm; d) 550 nm; e) 750 nm; f) 1000 nm. Note that the images are plotted using constant color palette to show the decay of the magnetic signal
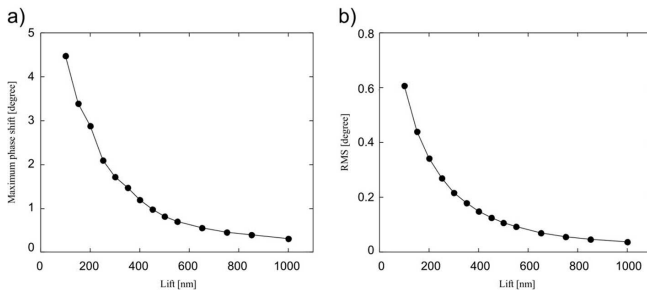

Fig. 7. Changes in the phase shifts (a), and RMS values of the phase shift variations as a function of the lift height
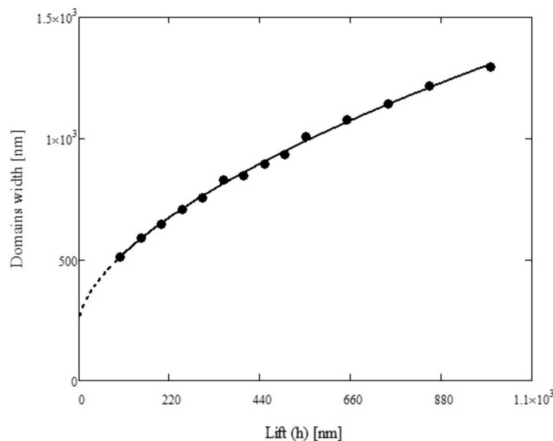

Fig. 8. Changes in FWHM widths vs. lift height (closed points) best fitted with the power function (solid line) and its extrapolation down to zero lift height (dotted line)

Fig. 8 presents variations in the FWHM widths of the autocorrealation function profiles measured vs. the lift height. In the range from 0.1 to 1.0 μm obtained results are best fitted by the power function written in the form:

$$y(h) = 18,47h^{0,59} + 232,6 \ [nm] \qquad (9)$$

By extrapolation, the above expression asymptotically goes to 232,6 nm with the lift height going to zero, which defines approximately the average width of the magnetic domain right on the surface.

Results of the fractal analysis of the magnetic signals are presented in Fig. 9, which exhibits significant dependence between previously mentioned fractal parameters (the fractal dimension D, the topothesis K, and the corner frequency τ_c), and the lift height value. Note that the changes in the fractal dimension are especially intriguing (Fig. 9a). In the beginning, the D value decreases with increasing lift height due to diminishing magnetic tip-surface interaction. As shown in Fig. 1, the decaying phase shift results from the diminished overlap of the stray magnetic fields the surface and that emitted by the probe's tip. The fractal dimension falls down from 1.191 for the lift height equal to 100 nm down to 0.966 for h = 400 nm, for which it takes the minimum value D_{min}. With the lift height increasing even further up to 1 mm, the fractal dimension systematically raises up to 1.45.

Note that the fractal dimension of surface structures D should fall somewhere between 1 and 2. However, our experiments at least partly resulted in D values slightly below unity for the lift heights in the range from 250 to 550 nm. Because the fractal dimension varies smoothly otherwise, we suggest that such an oddity might be specific of the measured signal, that is of the phase shift between the piezo drive and recorded cantilever vibrations. To confirm this assumption we analyzed an artificially generated sinusoidal signal, and obtained results are shown in Fig. 10. Using the same numerical procedure, the D value appeared to be 0.93, which agrees with our suggestion that the fractal dimension derived from the phase shift variations has a little to do with that calculated from topographical data because they are restricted to different limits.

In addition, presented results support previous findings [6, 9] that the fractal dimension is only slightly dependent on common statistical parameters such as those describing the arrangement of points on the surface: S_a, S_q, S_y. Here, substantial overlap of the magnetic fields at low lift heights yields large gradient, and the fractal dimension is dominated by the magnetic interactions. With the raising lift height, however, the magnetic forces steadily disappear leaving behind other interactions: thermal noises, long-range forces, or even dissipative forces (drag forces), which give rise to the residual tip-surface interactions.

After passing critical lift height (450 nm), for which $D = D_{min}$, increasing the tip-surface distance results in raising fractal dimension despite low magnetic forces (at the distance equal to 1 μm the residual magnetic interaction is approximately 15 times lower to that at h equal to 100 nm). On the contrary, plots in Fig. 9(b) and (c) clearly show that in the entire lift height range under study, the topothesy decays asymptotically towards zero, whereas the corner frequency behaves opposite – goes smoothly from a very small value up to about 1.8 μm.
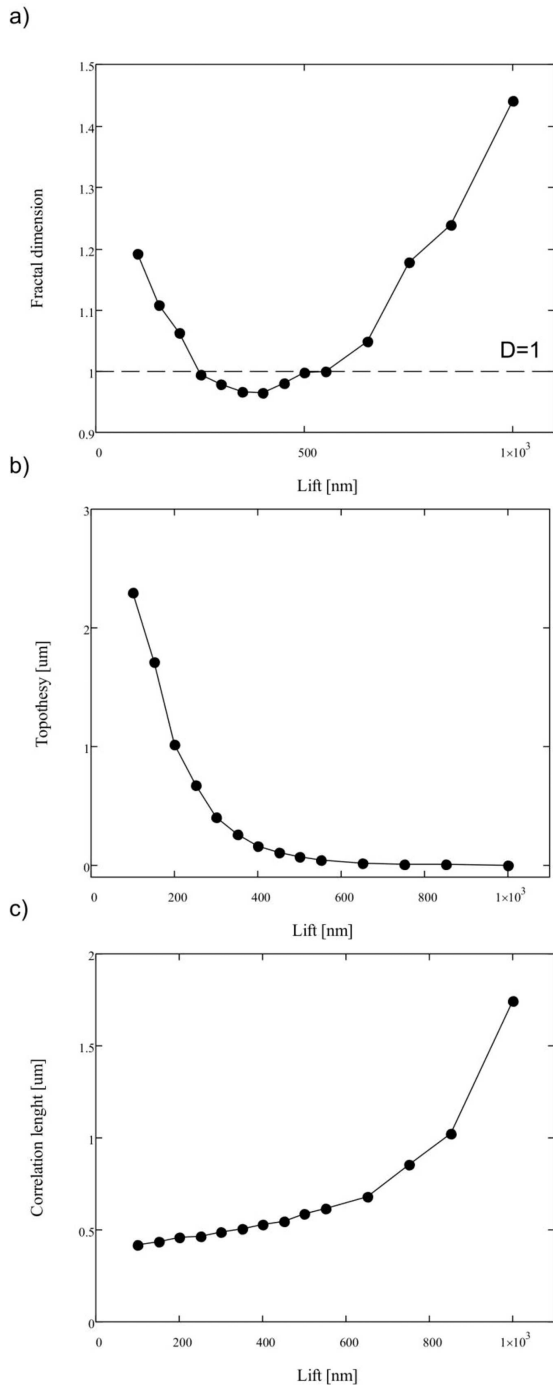
a)

b)

c)

Fig. 9. Changes in fractal parameters vs. the lift height: a) $D = f(h)$; b) $K = f(h)$4; c) $\tau_c = f(h)$
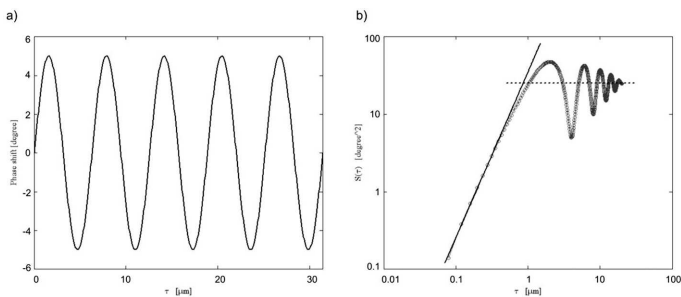
a)

b)

Fig. 10. Artificial profile of sinusoidal-type phase shift function for estimation of fractal parameters: (a) ideal phase shift, (b) log-log plot of the structure function

4. Conclusions

Performed research exhibits the dependence between the geometric and fractal parameters derived from MFM data and the lift height, at which the MFM imaging is carried out. This dependence occurs as an combined effect of the shape and the magnitude of magnetic stray field on one hand, and the overlap between the fields emitted by the surface and the tip on the other. The diameter of the magnetic domains on the studied surface was estimated by extrapolation of the values obtained at non-zero lift heights down to zero. The average domain diameter is found to be approximately 230 nm.

The dynamics of the tip-surface magnetic interactions along the normal was studied by considering variations in the fractal parameters derived from the structure function $S(\tau)$. All the fractal parameters, namely fractal dimension D, topothesy K, and corner frequency τ_c turned out to be dependent on the lift height, but the first one behaved differently from the rest. As expected, both the topothesy and the corner frequency exhibited regular dependence on the lift height, that is with asymptotically decaying magnetic interaction, but the fractal dimension evolved in a more complex manner. More specifically, this parameter initially decreased with increasing lift height, but at some point (referred to as the critical lift height h_{cr}) it approached the minimum value equal to 0.966 and started to raise afterwards. Unfortunately, any D value below 1 was previously believed forbidden for surface structures. Possible explanation makes use of the fact that the fractal dimension is computed from the phase shift signal between the cantilever and the piezo drive, which only indirectly probes the magnetic interaction. In fact, the phase shift exhibits the changes in the derivative of the magnetic force with respect to the position over the surface rather than the force itself, which might influence the whole picture. When the tip-surface distance raises far above the critical value, both the noise and residual non-magnetic interactions become significant in measured MFM signal.

On the whole, the method described in the paper establishes a measure of the critical lift height not to be exceeded for magnetic characterization of materials.

REFERENCES

[1] J.E. L e n n a r d - J o n e s, On the Determination of Molecular Fields, Proc. R. Soc. Lond. A **106** (738), 463-477 (1924).

[2] L. K o n g, S.Y. C h o u, Quantification of magnetic force microscopy using a micronscale current ring, Appl. Phys. Lett. **70** (15), 2043-2045 (1997).

[3] U. H a r t m a n n, An elementary introduction to atomic force microscopy and related methods, PDF document from the Institute of Experimental Physics, Univ. of Saarbrücken (www.uni-saarland.de/fak7/hartmann/download/afm/afm.pdf)

[4] R. P r o k s c h, K. B a b c o c k, J. C l e v e l a n d, Magnetic dissipation microscopy in ambient conditions, Appl. Phys. Lett. **74**, 419-421 (1999).

[5] P. G r u t t e r, Y. L i u, P. L e B l a n c, U. D u r i g, Magnetic dissipation force microscopy, Appl. Phys. Lett. **71**, 2, 279-281 (1997).

[6] E. M a i n s a h, J.A. G r e e n w o o d, D.G. C h e t w y n d, Metrology and Properties of Engineering Surfaces, Kluwer Academic Publishers (2001).

[7] K.J. S t o u t, P.J. S u l l i v a n, W.P. D o n g, E. M a i n s a h, N. L u o, T. M a t h i a, H. Z a h o u a n i, The development of methods for the characterisation of roughness in three dimensions, Publication no EUR15178EN of the Commission of the European Communities Dissemination of Scientific and Technical Knowledge Unit Directorate General Information Technologies and Industries and Telecommunications, University of Birmingham Edgbaston, Birmingham, B152 TT, 1993.

[8] M. B r a m o w i c z, S. K u l e s z a, A magnetic force microscopy study of magnetic domain structure in maraging steel, Solid State Phenomena – in press.

[9] J.C. R u s s, Fractal Sufaces, Plenum Press, New York (1994).

[10] J.J. W u, Analyses and simulation of anisotropic fractal surfaces, Chaos, Solitons and Fractals **13**, 1791-1806 (2002).